XII International Conference on Computational Plasticity. Fundamentals and Applications
COMPLAS XII
E. Oñate, D.R.J. Owen, D. Peric and B. Suárez (Eds)

C^1- CONTINUOUS CRACK PROPAGATION FOR MIXED-MODE FRACTURE PROBLEMS

A.T. Slobbe*, M.A.N. Hendriks*,†, J.G. Rots*

*Faculty of Civil Engineering and Geosciences, Delft University of Technology
P.O. Box 5048, 2600 GA Delft, The Netherlands
e-mail: a.t.slobbe@tudelft.nl (A.T. Slobbe)

†Norwegian University of science and technology (NTNU)
Rich. Birkelandsvei 1A, 7491 Trondheim, Norway

Key words: Crack propagation algorithm, Directional mesh bias, Quasi-brittle materials, Mixed-mode fracture

Abstract. In this work a C^1- continuous crack propagation algorithm is proposed to improve the numerical simulation of localized deformation patterns, using higher order elements. The algorithm is applied for a standard smeared crack model and is validated by a mixed-mode fracture problem. From the results a reduction of mesh-induced directional bias is observed.

1 INTRODUCTION

Crack tracking algorithms are used in various material models, e.g. [1, 2, 3], to capture localized deformation patterns with numerical simulations properly and to obtain mesh objective results. Within the framework of advanced X-FEM modeling the level set concept as tracking technique is even a key ingredient to describe the process of crack propagation. Since standard smeared crack approaches generally suffer to mesh-induced directional bias, enhancement with a crack tracking or propagation algorithm can be useful.

The main principle of a crack tracking algorithm is to trace and designate potential crack paths within an arbitrary finite element (FE) discretization. Elements crossed by a crack path are allowed to experience nonlinear material behavior. Elements outside the crack paths are restrained from that and keep their constitutive relation still linearly elastic.

Different types of algorithms exist, each with its own complexity of implementation, computational costs and robustness [4]. Recently, Cervera et al. [5] proposed an enhanced *local* crack tracking technique within the standard smeared damage approach. The algorithm, implemented in an incremental-iterative solution scheme, is relatively simple, computationally inexpensive and particularly suitable when meshes consisting of constant strain

triangular elements with one-point integration are used. From the results of numerical simulations of tension and mixed-mode cracking problems in quasi-brittle materials a clear elimination of directional mesh bias was observed.
In this work a new *local* crack tracking algorithm is presented, which is specifically developed for crack propagation in FE discretizations that consist of higher order quadratic elements with full numerical integration. Generally, these elements perform better in describing more complex deformation modes and failure modes, giving them a recommended position in guidelines for engineers [6]. In addition, quadratic elements serve the formulation of smooth curved cracking paths. The new proposed algorithm is applied for a classical smeared fixed crack model and is implemented in the Sequentially Linear Analysis (SLA) method, e.g. [7, 8, 9]. The SLA method replaces the standard incremental-iterative solution procedure by a series of scaled linear analyses. In every analysis a critical element is detected. A *critical element* is the element that contains the integration point with the largest stress - current strength ratio in the structure. Subsequently, a stepwise stiffness and strength reduction in that integration point is applied. For such discrete stiffness and strength reductions the nonlinear stress - strain relation needs to be approximated with a finite number of damage increments.

In the remaining of this paper the new proposed crack propagation algorithm is briefly explained and validated by the modeling of a mixed-mode fracture problem. The selected benchmarks are some of the well-known double-edge-notched (DEN) plain concrete specimens of Nooru-Mohamed. Mesh objectivity is studied by using a structured and an unstructured FE discretization, consisting of elements with quadratic interpolation.

2 PROPOSED CRACK PROPAGATION ALGORITHM

A detailed description of the new crack propagation algorithm is provided in another work of the authors [10]. Here only the main features are briefly presented.
The algorithm makes use of an element-label system, comparable to Cervera et al. [5], for the administration and updates of crack paths. Fig. 1(a) illustrates the different element labels. A crack path, indicated by the thick red line, is assumed to initiate only in elements with a label 'potential crack root element' that are located at the border of the structure. It is possible to exclude elements at the mesh boundaries from being a 'potential crack root element' by the specification of a nonzero value for a user-defined parameter r_{excl}.
Basically, the general task of a crack propagation algorithm in the SLA method is labeling, relabeling and unlabeling of elements after each linear analysis. The element-label update depends on the type of critical element or event. Three different types of events can be distinguished:

- crack path initiation;
- crack path localization;
- crack path propagation.

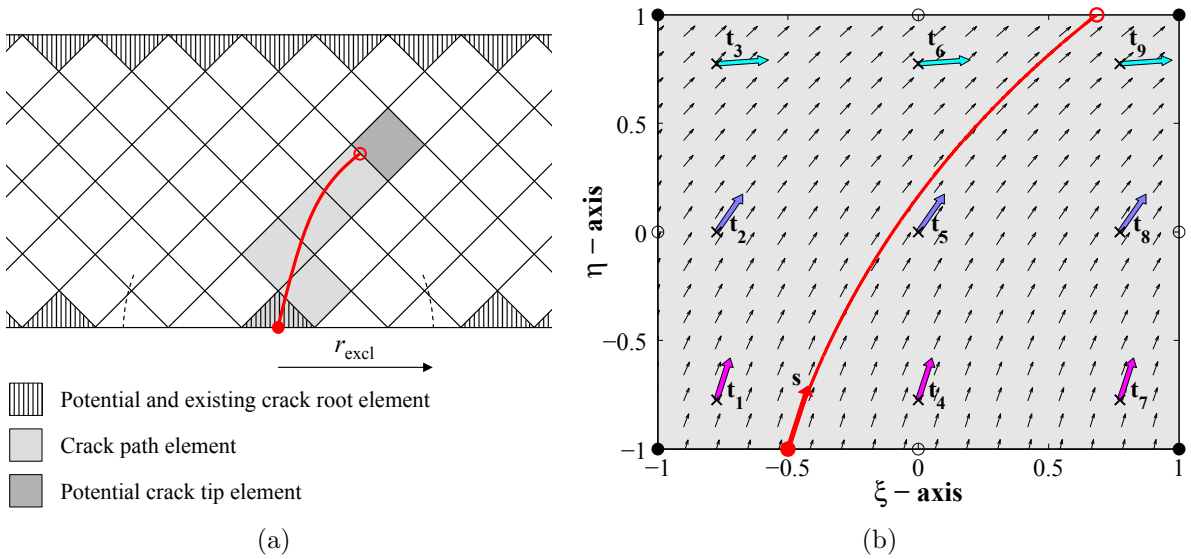

Figure 1: Element labels and definition r_{excl} in case of a single crack path (a) and a calculated crack propagation field with corresponding crack path for a 'potential crack *tip* element' with quadratic interpolation and full numerical integration (b).

Only labeled elements can become a critical element (see Section 1). Consequently, their integration points are allowed to experience nonlinear material behavior. Integration points in elements without a label do adopt a linear-elastic material behavior.
In case of the event 'crack path *localization*' an element with label 'crack path element' becomes critical. For this type of event no labeling, relabeling or unlabeling of elements is necessary. It only results in the update of material properties in the critical and either damaged or undamaged integration point. However, for the events 'crack path *initiation*' (if a 'potential crack root element' becomes critical) and 'crack path *propagation*' (if a 'potential crack tip element' becomes critical) an element-label update is required. Furthermore, in these two events a crack path propagation within the critical element needs to be derived. Note that the notion of crack path events matches well with the event driven nature of SLA. Consequently, no issues arise concerning prediction-correction strategies as in an incremental-iterative solution procedure.
Crack path propagation within a critical element is the key aspect of the new algorithm and is done in three subsequent steps. The procedure will be explained for crack path propagation through a 'potential crack tip element'. Fig. 1(b) shows a quadratic plane stress element with full numerical integration. The point where the crack path enters the element is indicated with the symbol '•'. In the first step the crack propagation angles are determined at all integration points. These angles are based on the maximum principal tensile stresses. Given a certain stress state, the corresponding normalized crack propagation vectors $\mathbf{t_1}$ - $\mathbf{t_9}$ in the nine points are depicted by means of colored arrows in a cyan-magenta color range. In the next step a linear crack propagation angle field within

the element is calculated. This is based on the crack propagation angles in the integration points and the propagation direction with which the crack track enters the element (red vector **s**). The contribution or influence of each integration point to the crack propagation angle field is made dependent on its principal stress values. In Fig. 1(b) this is indicated with the intensity of the cyan-magenta color. Magenta stands for a high contribution or influence on the crack direction field, where for the cyan color it is the opposite. By taking into account the propagation direction at the entry point explicitly, C^1- continuity of the crack path across the elements can be obtained. Finally, the crack propagation angle field is translated to a normalized crack propagation vector field (small black arrows). Starting from the bottom edge the crack path (curved red line) in the element is defined by a streamline and can subsequently be derived by going stepwise through the vector field until it again intersects with an element edge. The propagation direction at the exit point (symbol '○') is the propagation direction at the entry point of the new 'potential crack tip element' on the other side of the intersected edge, once that element becomes critical.

3 NUMERICAL SIMULATIONS OF DEN SPECIMENS

The plain concrete DEN specimens have been tested by Nooru-Mohamed [11], aiming for to broaden the knowledge of mixed-mode tensile cracking. Different load paths were applied on specimens with different sizes. In this paper only the specimens with dimensions of 200 mm × 200 mm × 50 mm, subjected to the nonproportional load path 4, are considered. These tests has been numerically simulated by several authors, e.g. [7, 12, 13, 14, 15]. Section 3.1 describes the experimental test setup and numerical modeling aspects. The results of the numerical simulations are presented in the Sections 3.2 - 3.4.

3.1 Modeling aspects

Fig. 2 shows the test setup and the geometry of the considered DEN specimens. The square shaped specimens with thickness of 50 mm were first subjected to a certain lateral shear force P_s, applied in displacement control. During this time the specimen was allowed to deform in vertical direction (so $P = 0$ kN). Subsequently, P_s was switched to load control and kept constant, and an axial tensile load P was applied under displacement control until failure. In case of load path 4 three different values for P_s were adopted: P_s = 5 kN (load path 4a, '48-03'), P_s = 10 kN (load path 4b, '46-05' and '47-01') and P_s = $P_{\mathrm{s;max}}$ = 27.5 kN (load path 4c, '47-06').
The numerical 'specimens' used in this section have been meshed by plane stress elements with sides of 5 mm. For the material behavior a smeared orthogonal fixed crack model and a variable shear retention relation have been adopted [9]. Regularization of the model is obtained by using the crack band approach [16]. The formulation of Govindjee et al. [17], based on Oliver [18], has been used to estimate the crack bandwidths in the

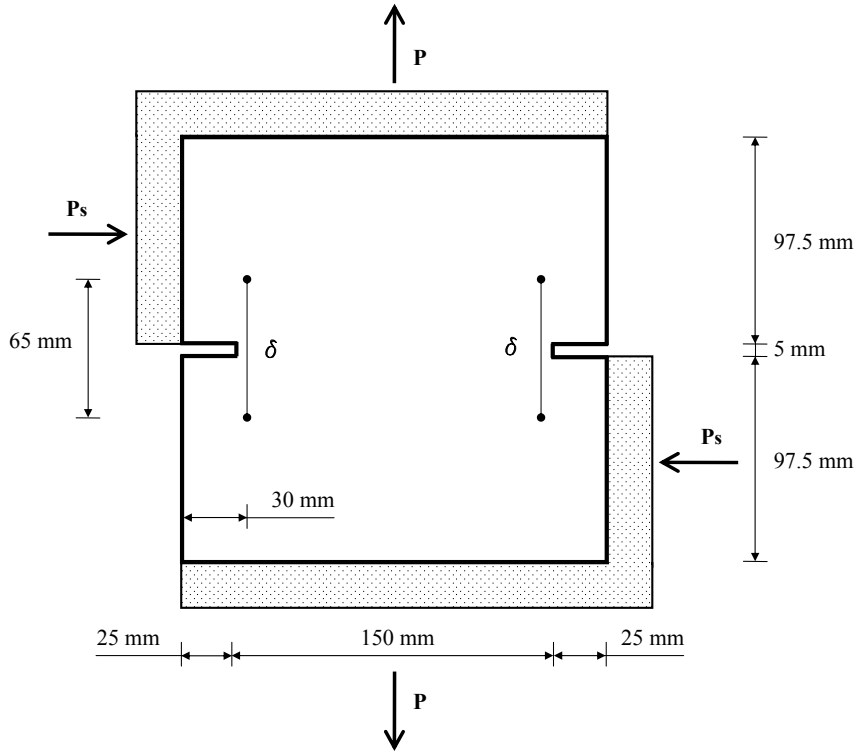

Figure 2: Geometry and experimental test setup of DEN specimens.

integration points. Assumed concrete material properties are: a Young's modulus E_0 of 30,000 N/mm^2, a tensile strength f_t of 3.0 N/mm^2, a material fracture energy G_f of 0.1 N/mm and a Poisson's ratio ν of 0.2. Furthermore, a nonlinear stress - strain relation according to Hordijk [19] has been used, discretized by 20 damage increments [9]. The corresponding crack opening w_{ult}, at which stresses can no longer be transferred along the crack, is equal to 0.171 mm.

For all three load paths sequentially linear analyses have been performed with and without the proposed crack propagation algorithm. Both a structured mesh of quadrilateral elements based on quadratic interpolation and using a 3×3 Gauss integration scheme, and an unstructured mesh of triangular elements based on quadratic interpolation and using 3-point Gauss integration have been adopted. So, in total twelve numerical analyses have been performed, four for each load path. In case the crack propagation algorithm has been used, the parameter r_{excl} is put on 0.

The results of all numerical analyses have been assessed by considering the global behavior in terms of load P versus $\delta_{average}$. The $\delta_{average}$ is the mean value of the two measured δ's shown in Fig. 2. Furthermore, the obtained damage contours (and some crack patterns) after failure are considered. These contours are plotted in a deformed mesh with a displacement amplification factor equal to 100.

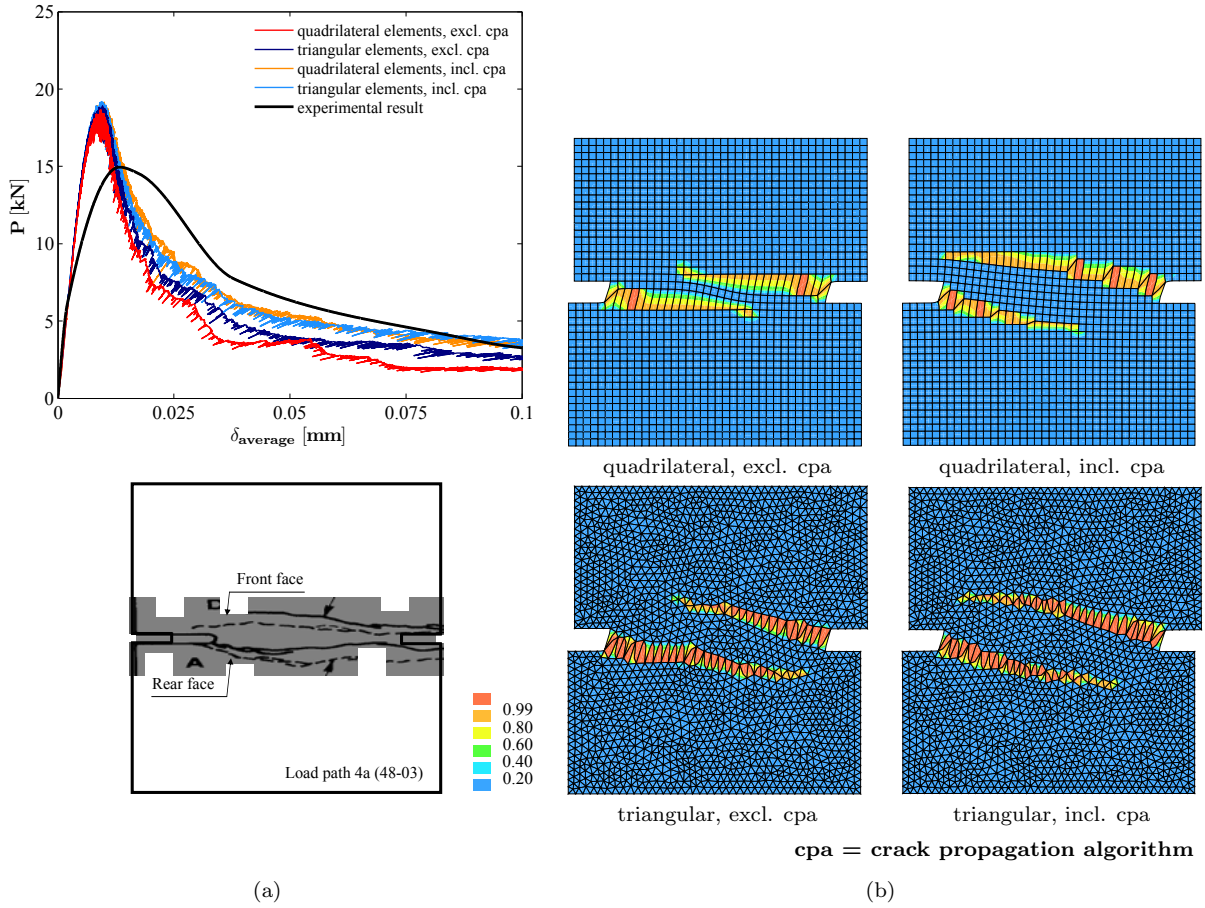

Figure 3: P - δ_{average} responses of analyses on DEN specimen - load path 4a, experimental crack pattern (a) and corresponding damage contours at $\delta_{\text{average}} = 0.1$ mm in deformed meshes ($\times 100$) (b).

3.2 Load path 4a

In load path 4a the specimen was subjected to an initial shear force P_{s} of 5 kN. Fig. 3(a) shows the graphs with the P - δ_{average} responses of the four analyses. The experimentally obtained P - δ_{average} response (thick black line) and failure crack pattern of specimen '48-03' are also depicted. The damage contours at $\delta_{\text{average}} = 0.1$ mm of the four analyses are given in Fig. 3(b).

From the graph it can be observed that the numerically obtained curves are in good agreement with each other. Reasonable agreement with the experimental curve can be noticed. However, considering the failure load of the experimental test, a significant overestimation is visible. Similar overestimations were also reported by some of the referred authors at the beginning of Section 3, whereas others changed the material properties to decrease the peak load. The overestimation could be a result of unintended deficiencies in the experimental test setup [12] that are not incorporated in the FE model.

All the numerically obtained damage contours reveal two distinct cracks, as seen in the

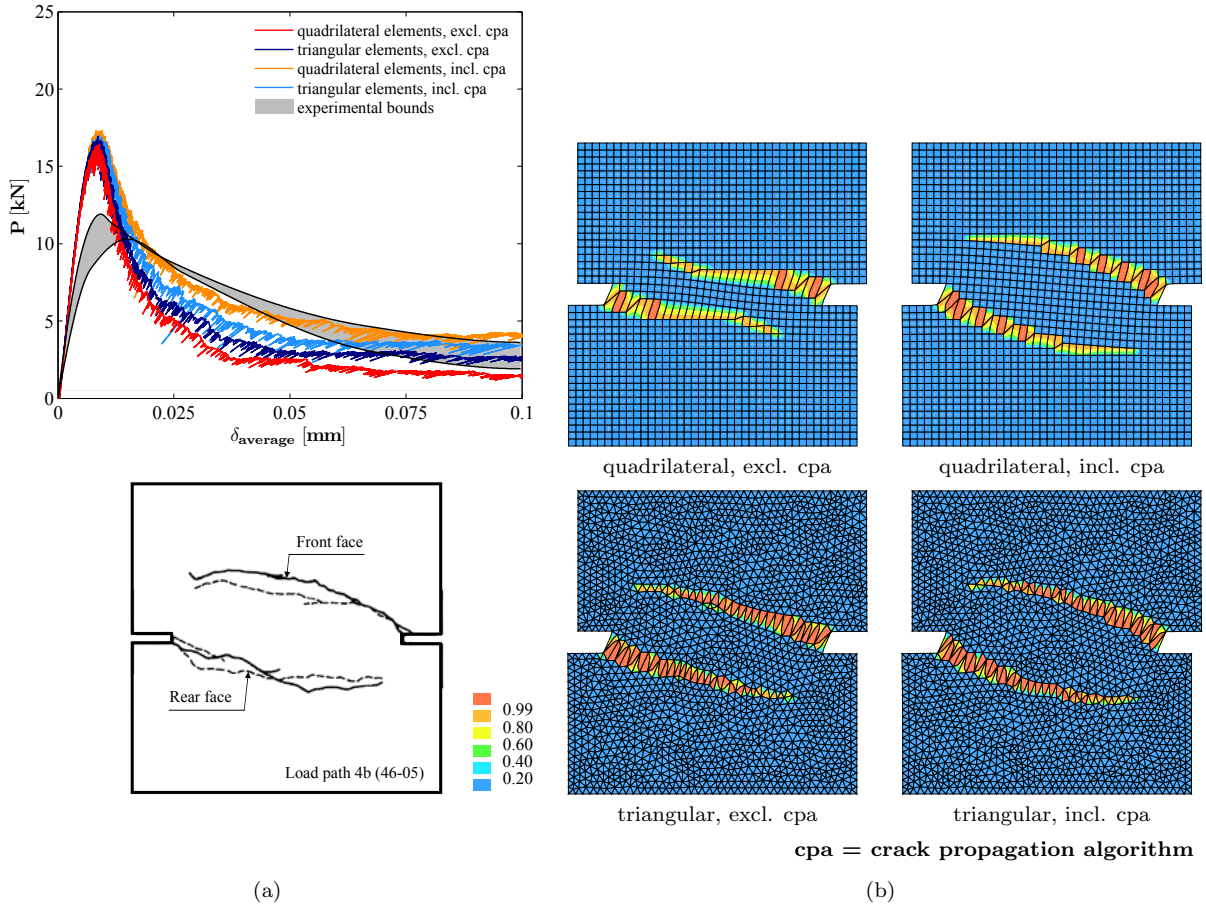

Figure 4: P - δ_{average} responses of analyses on DEN specimen - load path 4b, experimental crack pattern (a) and corresponding damage contours at $\delta_{\text{average}} = 0.1$ mm in deformed meshes ($\times 100$) (b).

experiment. The crack patterns of the analyses without the proposed crack propagation algorithm (cpa) show some differences with each other. Addition of the algorithm results in approximately identical crack patterns, indicating objectivity to the mesh orientation.

3.3 Load path 4b

For load path 4b an initial shear force P_{s} of 10 kN was applied. The corresponding experimental results and numerical output is shown in Fig. 4. The global response from the experimental test is indicated with a gray shaded area, since two specimens ('46-05' and '47-01') were subjected to this load path. Although these P - δ_{average} results reveal some scatter, the observed crack patterns were similar for both specimens [15].
The graph in Fig. 4(a) shows the numerical P - δ_{average} responses. Again, good agreement between these four curves exist. Although the experimental failure load is still significantly overestimated, the heights of the numerically obtained peak values are lower than the ones in Fig. 3(a). This indicates that the experimentally observed trend of 'decreasing

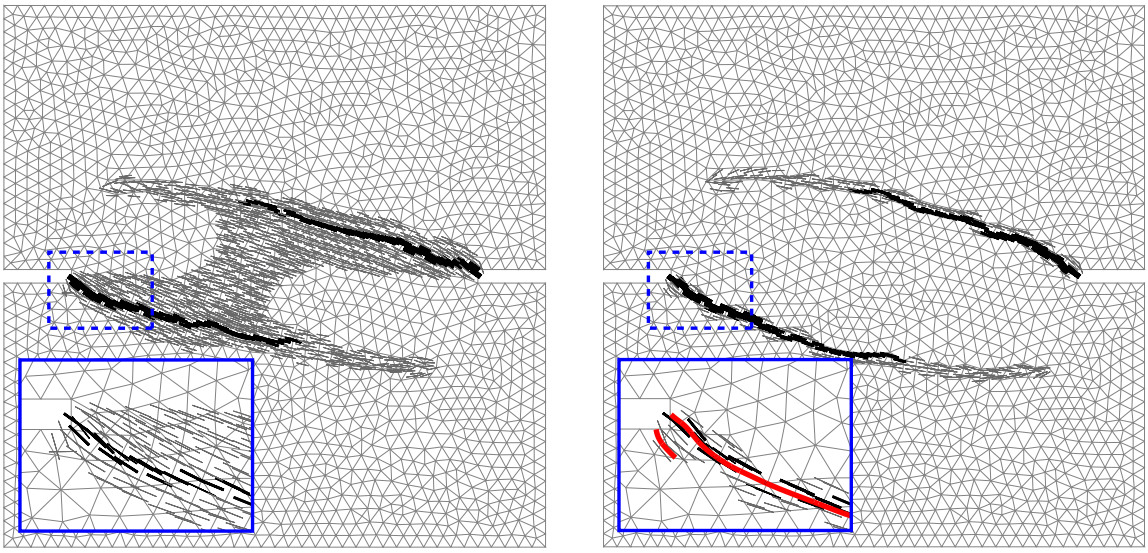

triangular, excl. crack propagation algorithm
(a)

triangular, incl. crack propagation algorithm
(b)

Figure 5: Crack width plots at $\delta_{\text{average}} = 0.1$ mm belonging to analyses on DEN specimen - load path 4b with unstructured mesh. The thickest black lines correspond to $w \geq w_{\text{ult}}$. The red line indicates the C^1- continuous crack path.

P_{peak} by increasing P_{s}' is captured well.
The damage contours in Fig. 4(b) reveal again no mesh-induced directional bias when the crack propagation algorithm (cpa) is adopted. Both plots are point symmetric with respect to the specimen's midpoint and show two curved cracks that are similarly shaped to the experimentally obtained failure cracks. For the analyses without the proposed algorithm only in case of the unstructured mesh with quadratic triangular elements the failure crack pattern is reasonable well predicted. The two macro cracks are just somewhat less curved. In case of the structured mesh, consisting of squared quadrilaterals, the macro crack development clearly suffers to mesh alignment, i.e. the tendency for crack propagation along continuous mesh lines.
Interesting to note is that a relation can be observed between the curvatures of the macro cracks in the damage contours and the height of the residual loads at $\delta_{\text{average}} = 0.1$ mm in the P - δ_{average} graph. The more curvature, the higher the residual load P (although all of them remain in an acceptable range). This trend, also noticed in the numerical results of other load paths, can be attributed to the phenomenon of stress locking [20].
Fig. 5 shows the crack patterns at $\delta_{\text{average}} = 0.1$ mm of the analyses with an unstructured mesh. The local cracks in the integration points are plotted with three different linewidths, indicating the increasing crack widths in the three ranges $\langle 0, 1/2\, w_{\text{ult}} \rangle$, $[1/2\, w_{\text{ult}}, w_{\text{ult}} \rangle$, $[w_{\text{ult}}, \rightarrow \rangle$. In case of no crack propagation algorithm a lot of spurious cracks between the two curved macro cracks can be observed. From the corresponding damage contour in Fig. 4(b) it can be concluded that most of these cracks hardly dissipate energy.

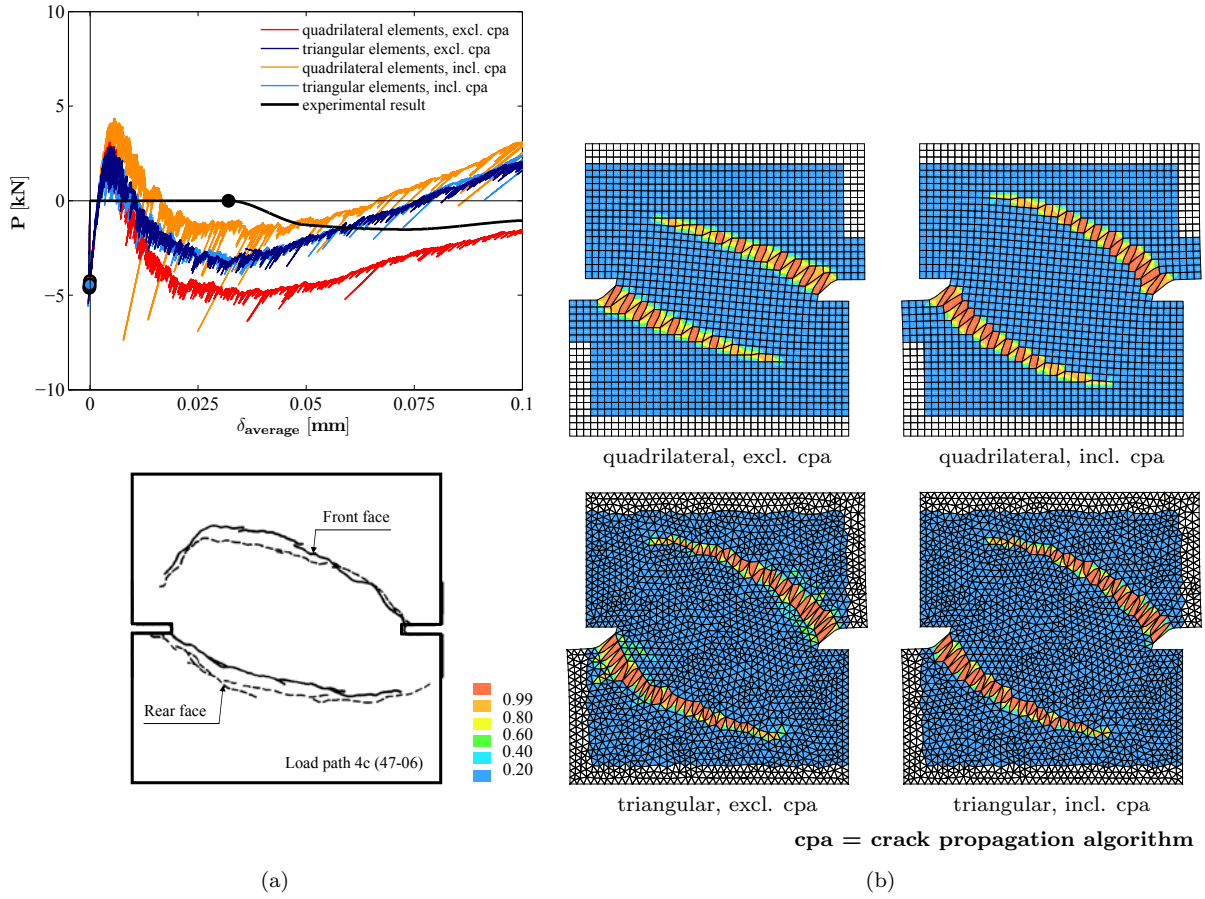

Figure 6: P - δ_{average} responses of analyses on DEN specimen - load path 4c, experimental crack pattern (a) and corresponding damage contours at $\delta_{\text{average}} = 0.1$ mm in deformed meshes ($\times 100$) (b).

Details of the crack patterns around the left notch of the specimen are provided by the small pictures in the blue rectangles. For the analysis including the proposed algorithm the corresponding crack paths are added (red lines). The smoothness of the lines indicates that C^1- continuity is indeed obtained.

3.4 Load path 4c

The tested specimen '47-06', belonging to load path 4c, was initially loaded by $P_{\text{s}} = P_{\text{s;max}}$, which was found to be equal to 27.5 kN. Experimentally and numerically obtained P - δ_{average} responses and failure crack patterns are given in Fig. 6. Before discussing the results it should be noted that for the elements in the bottom-left and top-right corners a linear-elastic material behavior is adopted, see the white colored elements in Fig. 6(b). This 'trick' is done to prevent failure by horizontally propagating cracks in these regions. Both in the experiments and in numerical analyses such a failure mode has been observed [13, 15].

The P - δ_{average} graph in Fig. 6(a) reveals considerable differences between the experimental and numerical curves. The main reason for this is caused by incorrect applied boundary conditions. For simplification the vertical constraints, needed to apply the displacement controlled P in the second loading stage, were also present during the initial shear loading stage. Contrary to the experiment (see description in Section 3.1) this does not allow for free vertical deformation of the specimen during P_{s} was applied. Consequently, the moment that the axial tensile load P was activated (indicated with the plotted dots in the graph) is not at $P = 0$ kN and $\delta_{\text{average}} > 0$ mm, but at $P < 0$ kN and $\delta_{\text{average}} = 0$ mm. The authors realize that above simplification affect the results, but since this paper is mainly focused on the validation of the proposed algorithm the numerical analyses can be still valuable. Note that these issues do not play a role in case of load paths 4a and 4b. The experimental results of these tests show that no vertical deformations during the initial shear loading stage occurred [11].
From a qualitative comparison between the numerical and experimental curves reasonable agreement can be observed. The numerical curves show with an increasing δ_{average} that the axial load P becomes a compression load. In a later stage the compression load decreases again. Both phenomena were also visible in the experiment.
Regarding the damage contours at $\delta_{\text{average}} = 0.1$ mm in Fig. 6(b), it can be seen that also in case of load path 4c the analyses including the crack propagation algorithm (cpa) do not suffer to directional mesh bias. This is not true for the analyses without the algorithm, where in the structured mesh the macro cracks are less curved. Except for this one, the predicted failure crack patterns are generally in good agreement with the experimental result. None of the analyses was able to capture the drastic change in curvature at the end of the experimental top macro crack.

4 CONCLUSIONS

This paper briefly presents a new crack propagation algorithm that is specifically aimed to be used in combination with higher order elements. The proposed algorithm is validated on double-edge-notched plain concrete specimens of Nooru-Mohamed. Three different load paths of this mixed-mode fracture problem are analyzed. Based on the results the following conclusions can be drawn:

- Enhancement of the smeared fixed crack model by the proposed algorithm leads to an improvement of the mesh objectivity, i.e. the mesh-induced directional bias is reduced.

- The crack propagation algorithm is especially relevant for structured meshes, consisting of quadrilaterals.

- The proposed algorithm avoids spurious cracking and enables to obtain C^1- continuous crack paths within FE discretizations.

REFERENCES

[1] Cervera, M., Chiumenti, M. Mesh objective tensile cracking via a local continuum damage model and a crack tracking technique. *Computer Methods in Applied Mechanics and Engineering* (2006) **196**:304-320.

[2] Oliver, J., Huespe, A.E. Continuum approach to material failure in strong discontinuity settings. *Computer Methods in Applied Mechanics and Engineering* (2004) **193**:3195-3220.

[3] Stolarska, M., Chopp, D.L., Moës, N., Belytschko, T. Modelling crack growth by level sets in the extended finite element method. *International Journal for Numerical Methods in Engineering* (2001) **51**:943-960.

[4] Jäger, P., Steinmann, P., Kuhl, E. Modeling three-dimensional crack propagation - A comparison of crack path tracking strategies. *International Journal for Numerical Methods in Engineering* (2008) **76**:1328-1352.

[5] Cervera, M., Pela, L., Clemente, R., Roca, P. A crack-tracking technique for localized damage in quasi-brittle materials. *Engineering Fracture Mechanics* (2010) **77**:2431-2450.

[6] The Dutch ministry of public works and the environment. *Guidelines for Nonlinear Finite Element Analysis of Concrete Structures. Scope: Girder Members.* Document RTD 1016:2012 (2012).

[7] DeJong, M.J., Hendriks, M.A.N., Rots, J.G. Sequentially linear analysis of fracture under non-proportional loading. *Engineering Fracture Mechanics* (2008) **75**:5042-5056.

[8] Rots, J.G., Belletti, B., Invernizzi, S. Robust modeling of RC structures with an 'event-by-event' strategy. *Engineering Fracture Mechanics* (2008) **75**:590-614.

[9] Slobbe, A.T., Hendriks, M.A.N., Rots, J.G. Sequentially linear analysis of shear critical reinforced concrete beams without shear reinforcement. *Finite Elements in Analysis and Design* (2012) **50**:108-124.

[10] Slobbe, A.T., Hendriks, M.A.N., Rots, J.G. A C^1- continuous crack propagation algorithm for the modeling of localized damage with higher order quadratic elements. *To be submitted.*

[11] Nooru-Mohamed, M.B. *Mixed-mode fracture of concrete: an experimental approach.* PhD, Delft University of Technology (1992).

[12] Cervera, M., Chiumenti, M. Smeared crack approach: back to the original track. *International Journal for Numerical and Analytical Methods in Geomechanics* (2006) **30**:1173-1199.

[13] di Prisco, M., Ferrara, L., Meftah, F., Pamin, J., de Borst, R, Mazars, J., Reynquard, J.M. Mixed mode fracture in plain and reinforced concrete: some results on benchmark tests. *International Journal of Fracture* (2000) **103**:127-148.

[14] Jirasek, M., Grassl, P. Evaluation of directional mesh bias in concrete fracture simulations using continuum damage models. *Engineering Fracture Mechanics* (2008) **75**:1921-1943.

[15] Nooru-Mohamed, M.B., Schlangen, E., Mier, van, J.G.M. Experimental and numerical study on the behavior of concrete subjected to biaxial tension and shear. *Advanced Cement Based Materials* (1993) **1**:22-37.

[16] Bazant, Z.P., Oh, B.H. Crack band theory for fracture of concrete. *Material and Structures* (1983) **16**:155-177.

[17] Govindjee, S., Kay, G.J., Simo, J.C. Anisotropic modelling and numerical simulation of brittle damage in concrete. *International Journal for numerical Methods in Engineering* (1995) **38**:3611-3633.

[18] Oliver, J. A consistent characteristic length for smeared cracking models. *International Journal for numerical Methods in Engineering* (1989) **28**:461-474.

[19] Hordijk, D.A. *Local approach to fatigue of concrete*. PhD, Delft University of Technology (1991).

[20] Rots, J.G. *Computational modeling of concrete fracture*. PhD, Delft University of Technology (1988).